J. Biochem. **137**, 587–592 (2005)
DOI: 10.1093/jb/mvi078

Structural Basis for Thermostability of Endo-1,5-α-L-Arabinanase from *Bacillus thermodenitrificans* TS-3

Asako Yamaguchi[1], Toshiji Tada[1,*], Kei Wada[1], Tetsuko Nakaniwa[1], Tomoya Kitatani[1], Yuri Sogabe[1], Makoto Takao[2], Takuo Sakai[2] and Keiichiro Nishimura[1]

[1]Research Institute for Advanced Science and Technology, Osaka Prefecture University, Sakai, Osaka 599-8570; and [2]IGA Bioresearch, Amagasaki, Hyogo 660-0805

Received December 10, 2004; accepted February 21, 2005

The crystal structure of a thermostable endo-1,5-α-L-arabinanase, ABN-TS, from *Bacillus thermodenitrificans* TS-3 was determined at 1.9 Å to an *R*-factor of 18.3% and an *R*-free-factor of 22.5%. The enzyme molecule has a five-bladed β-propeller fold. The substrate-binding cleft formed across one face of the propeller is open on both sides to allow random binding of several sugar units in the polymeric substrate arabinan. The β-propeller fold is stabilized through a ring closure. ABN-TS exhibits a new closure-mode involving residues in the N-terminal region: Phe7 to Gly21 exhibit hydrogen bonds and hydrophobic interactions with the first and last blades, and Phe4 links the second and third blades through a hydrogen bond and an aromatic stacking interaction, respectively. The role of the N-terminal region in the thermostability was confirmed with a mutant lacking 16 amino acid residues from the N-terminus of ABN-TS.

Key words: arabinanase, crystal structure, endo-acting enzyme, glycoside hydrolase, thermostability.

Abbreviations: ABN, 1,5-α-L-arabinanase; ABF, α-L-arabinofuranosidase; GH, glycoside hydrolase.

Arabinan is distributed in hemicelluloses, which comprise a large fraction of plant cell walls. The backbone of arabinan consists of linearly 1,5-linked α-arabinofuranosyl-residues, some of which are substituted with α-1,2- and α-1,3-linked side chains of L-arabinose in the furanose conformation (*1*). Two major enzymes that hydrolyze highly branched polysaccharides of arabinan are 1,5-α-L-arabinanases (ABNs; EC 3.2.1.99) and α-L-arabinofuranosidases (ABFs; EC 3.2.1.55). ABN enzymes, which are members of glycoside hydrolase (GH) family 43 (*2*, *3*), hydrolyze α-1,5-L-arabinofuranoside linkages. ABF enzymes, which are members of GH families 43, 51, 54 and 62 (*4*), cleave arabinose side chains. The combined actions of these two enzymes reduce arabinan to L-arabinose and/or arabinooligosaccharides (*5*).

L-Arabinose can be used as a bioactive non-calorie sweetener, because this sugar is poorly absorbed by the intestine and inhibits its sucrase to suppress an increase in the plasma glucose level (*6*). A large amount of L-arabinose is contained in agricultural waste, such as sugar beet pulp, wheat bran, rice bran, corn fibres, citrus peel and so on, and is not used much. Arabinan-degrading enzymes are invaluable in the food industry for the efficient production of L-arabinose from this agricultural waste. Thermostable arabinanases, which are stable and effective at high temperatures, are industrially important for the production of L-arabinose.

Recently, Takao *et al*. (*7*) isolated an interesting gene from *Bacillus thermodenitrificans* strain TS-3 that encodes a novel and thermostable endo-1,5-α-L-arabinanase, ABN-TS. ABN-TS comprises 312 amino acids and has a molecular weight of 35 kDa. ABN-TS hydrolyzes linear arabinan almost exclusively to arabinobiose through an endo mechanism and shows optimal activity at 343 K (*8*). Protein functions are governed by a fine balance between the stability and flexibility of proteins. Although the roles of these factors in biological functions are not well understood, recent studies (*9*, *10*) have indicated that a significant increase in stability is achieved in proteins from mesophiles on the inclusion of "rigidifying" mutations. Proteins are made rigid by deleting or shortening of loops (*11*), and also by increasing hydrophobic interactions, ion pairs, hydrogen bonds and disulfide bridges (*12*, *13*).

The crystal structure of α-L-arabinanase Arb43A from *Cellvibrio japonicus*, which exhibits both exo- and endo-modes of action, was determined by X-ray crystallography at a resolution of 1.9 Å (*14*). However, the three-dimensional structure of an endo-acting arabinanase has yet to be reported. Thus, we have conducted X-ray diffraction analysis of the thermostable and endo-acting arabinanase ABN-TS (*15*). To extend our study, we determined the structure of the enzyme to determine the features responsible for its thermostability and activity. We also prepared an ABN-TS mutant to confirm the importance of the N-terminal for the thermostability.

MATERIALS AND METHODS

Crystallization and Data Collection—Recombinant ABN-TS was overexpressed in *B. subtilis* MI112 (*7*) and purified. The purified ABN-TS was crystallized by the hanging-drop vapor-diffusion method using 1.0 M sodium citrate as a precipitant at pH 6.0. The purification, crys-

*To whom correspondence should be addressed. Phone: +81-72-254-9820, Fax: +81-72-252-6776, E-mail: tada@b.s.osakafu-u.ac.jp

Table 1. **Summary of data-collection and refinement statistics.**[a]

Data collection statistics[b]	
X-ray source	SPring-8, BL40B2
Wavelength (Å)	0.9
Temperature (K)	100
Resolution (Å)	1.9 (1.97–1.90)
Space group	$P2_12_12_1$
Unit-cell parameters (Å)	a = 40.3, b = 77.8, c = 89.7
R_{merge} (%) [c]	8.6 (27.6)
$I/\sigma(I)$	10.5 (2.4)
Number of observed reflections	170,121
Number of unique reflections	22,893
Completeness (%)	99.2 (96.5)
Mosaicity (°)	0.7
Refinement statistics	
Resolution (Å)	30–1.9
R-factor (%) [d]	18.3
R-free-factor (%) [e]	22.5
rmsd (bond distance) (Å)	0.006
rmsd (bond angle) (deg.)	1.4
Average B value (Å^2)	22.4
Ramachandran plot	
Most favored region (%)	81.7
Additionally allowed regions (%)	16.8
Generously allowed regions (%)	1.5
Disallowed regions (%)	0.0

[a]The values for the highest resolution shell (1.97–1.90 Å) are given in parentheses. [b]From Ref. *15*. [c]$R_{merge} = \Sigma_{hkl} \mid I - \langle I \rangle \mid / \Sigma_{hkl} \langle I \rangle$. [d]$R$-factor = $\Sigma \mid\mid F_{obs} \mid - \mid F_{calc} \mid / \Sigma \mid F_{calc} \mid$. [e]$R$-free-factor was calculated using 10% of the data.

tallization and data collection were reported previously (*15*). For data collection, the crystals were loop-mounted in a cryoprotectant solution containing 28% (*w*/*v*) sucrose and 1.0 M sodium citrate (pH 6.0), and then flash-cooled. A data set was successfully collected at 100 K using synchrotron radiation of 0.9 Å at the BL40B2 station of SPring-8. The crystals belong to orthorhombic space group $P2_12_12_1$, with unit cell parameters of a = 40.3, b = 77.8, and c = 89.7 Å. The data were processed with DENZO and SCALEPACK software (*16*).

Structure Determination and Refinement—The structure of ABN-TS was solved by the molecular replacement method with program AMoRe (*17*) implemented in the CCP4 suite (*18*). The structure of α-L-arabinanase Arb43A from *C. japonicus* (which exhibits 46% similarity to ABN-TS) (*14*) was used as a search model. A clear solution of translation function was obtained in the case of space group $P2_12_12_1$ with a correlation factor of 35.2 and an R-factor of 47.3%. Subsequently, refinement was performed by the simulated rigid-body positioning, annealing method, positional and individual B-factor refinements with program CNS (*19*), and manual rebuilding of the structure in O (*20*). After several rounds of refinement and model building, the R-factor and R-free-factor were reduced to 25.0 and 28.8%, respectively. Water molecules were added to the model at locations with $F_o - F_c$ densities higher than 3σ and hydrogen-bonding stereochemistry using the water-pick function of CNS. One peak exhibiting electron-density higher than 7σ was assigned to a chloride ion in the axial cavity. The final R-factor and R-free-factor were 18.3 and 22.5%, respectively. The stereochemistry of the final model was analyzed with program PROCHECK (*21*). The data collection and final refinement statistics are summarized in Table 1. The coordinates and structure factors have been deposited in the RCSB Protein Data Bank under accession code 1WL7.

Preparation and Characterization of an N-Terminal Deleted Mutant—A gene mutant lacking 16 amino acid residues at the N-terminus of ABN-TS was amplified by PCR using plasmid pUBabn containing the ABN-TS gene (*7*) as a template with the following primers: sense, 5′-TACGAAGGATCCATGAGTCTTAAGGGAG-3′; antisense, 5′-TTTTTGAAGCTTTTACAAATACGGCCACCC-3′. The PCR fragment was inserted into the *Bam*HI–*Hin*dIII sites of pUC18 (Takara) to construct a new plasmid, pUCTSnd. The sequence of pUCTSnd was verified by DNA sequencing with a dye terminator cycle sequencing kit (Beckman Coulter) and a CEQ2000 fragment analysis system (Beckman Coulter). The ABN-TS mutant was expressed in *Escherichia coli* JM109. *E. coli* JM109 harboring pUCTSnd was cultured in 1 liter of LB medium containing 100 μg/ml ampicillin at 310 K. Expression was induced by the addition of 0.5 mM isopropyl β-D-thiogalactopyranoside when the absorbance at 600 nm reached 0.5, and cultivation was continued for a further 5 h at 310 K. The cells were harvested, resuspended in 30 ml of 20 mM Tris-HCl, pH 8.0, and then sonicated. The cellular debris was removed by centrifugation, and the supernatant was purified by chromatography on DEAE Sepharose, Phenyl Sepharose (Amersham Biosciences), UNO-Q (Bio-Rad), and Superdex 200 (Amersham Biosciences) columns using an FPLC system from Amersham Biosciences at 277 K. The fractions containing ABN activity were pooled and dialyzed against 20 mM Tris-HCl buffer, pH 7.5.

The ABN activity was measured in a mixture comprising 200 μl of 0.5% debranched arabinan (Megazyme International) in 100 mM acetate buffer, pH 6.0, and 10 μl of an appropriately diluted enzyme solution, with incubation at 343 K for 30 m (*8*). The activity was determined by measuring the release of reducing groups by the method of Somogyi (*22*). The optimal temperature of the mutant was examined by measurements at temperatures ranging from 313 to 353 K. The optimal pH was examined in the pH range of 4.0 to 8.0.

Thermostability Measurements—The wild type enzyme was incubated at 343 K, and the mutant at 333 K and 338 K. An aliquot of each solution was removed and cooled on ice. The residual ABN activity was determined under the optimized conditions described above.

RESULTS AND DISCUSSION

Description of the ABN-TS Structure—The final model comprises all 312 amino acids of mature ABN-TS, one chloride ion and 240 water molecules. The structure of the ABN-TS molecule is shown in Fig. 1. The enzyme has a β-propeller fold consisting of five β-sheets, called blades, each of which is made up of four β-strands in an antiparallel arrangement. The β-sheets are twisted and radially arranged around the pseudo five-fold axis such

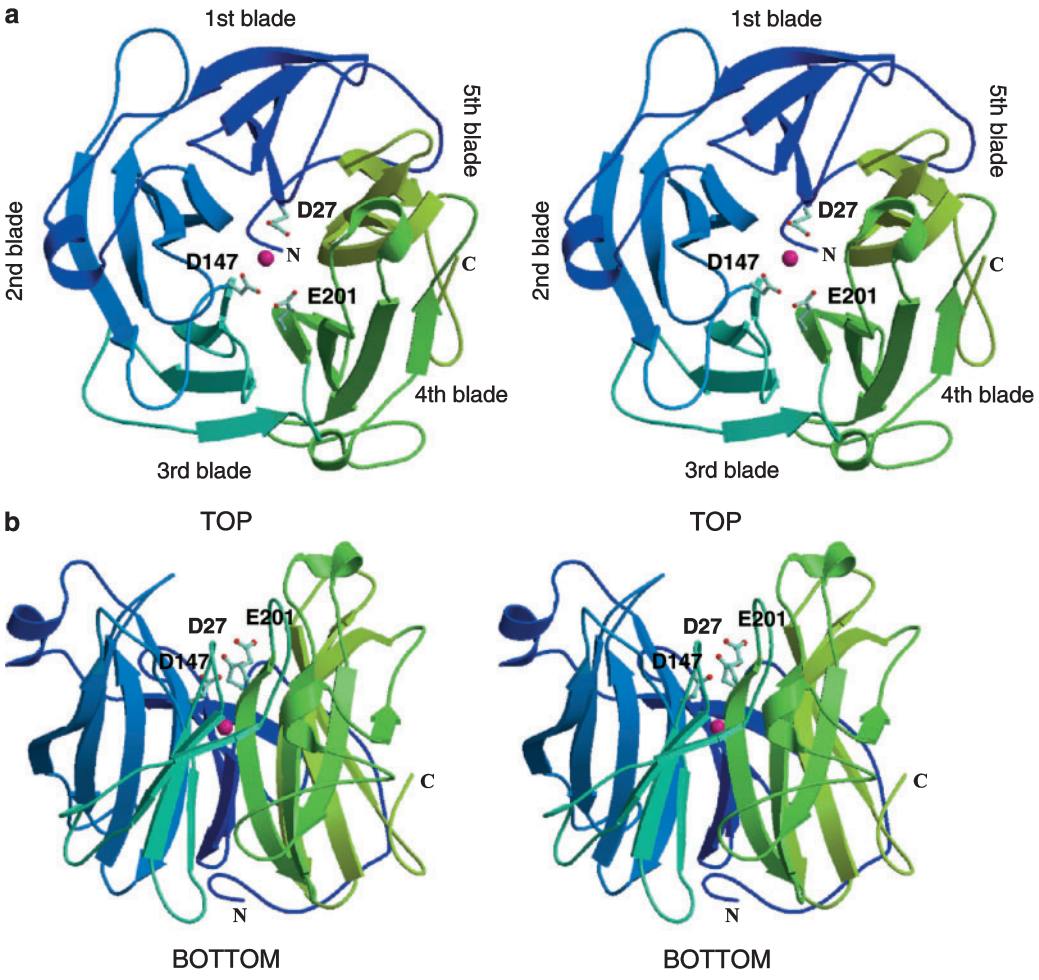

Fig. 1. **Stereoviews of ABN-TS shown as a ribbon diagram.** Each blade is shown in a different color. The chloride ion is shown as a magenta sphere. Three acidic residues, Asp27, Asp147 and Glu201, are shown as a ball-and-stick model. The substrate-binding cleft is located at the top of the molecule (b). These figures were drawn using programs MOLSCRIPT (*23*) and Raster3D (*24*).

that they pack face-to-face. The topology of ABN-TS is very similar to that of Arb43A as a whole.

A large cavity is elongated along the pseudo five-fold axis of the β-propeller fold. One peak exhibiting electron-density higher than 7σ was found in the cavity. The peak was surrounded by six water molecules and the $N\varepsilon_2$ atom of His271 in a pentagonal bipyramidal coordination with distances of 2.6–2.8 Å (Fig. 2). The enzyme was crystallized at pH 6.0 (*15*), so the side-chain of the histidine residue could be positively charged. Thus, we further refined the structure by considering that this site is occupied by a chloride ion (Fig. 1). The $F_o - F_c$ map did not show a positive peak when a chloride ion was assigned to this site. The chloride ion is considered to be taken up from the solution used for crystallization.

A pronounced substrate-binding cleft is formed across one face of the propeller, called the "top," while the other face, called the "bottom," is virtually flat, as shown in Fig. 1b. The cleft is characterized by three acidic residues, Asp27, Asp147 and Glu201, in the first, third and fourth blades, respectively. These residues are conserved at equivalent positions in all of the enzymes belonging to GH families 32, 43, 62 and 68 (*26*).

The Substrate-Binding Cleft—There is a significant difference in the structures of the substrate-binding clefts of ABN-TS and Arb43A (Fig. 3). The substrate-binding cleft of Arb43A, which exhibits exo and endo

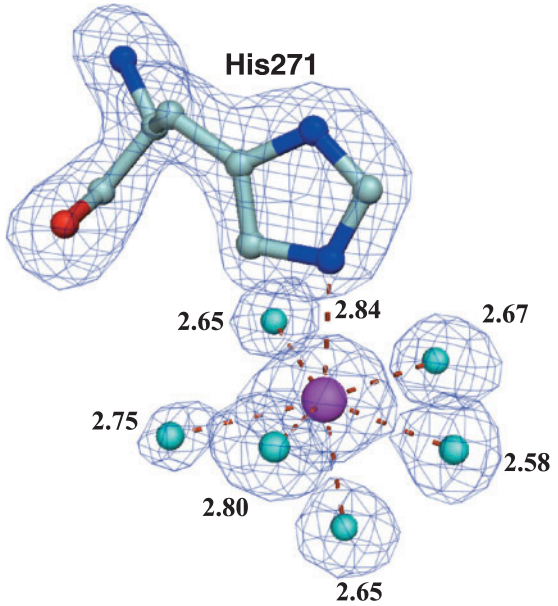

Fig. 2. **The environment around the chloride ion.** The positive electron difference densities were contoured at 4σ. The chloride ion is shown as a magenta sphere and the water molecules as cyan spheres. The ligand distances are given in Å. This figure was drawn using program DINO (*25*).

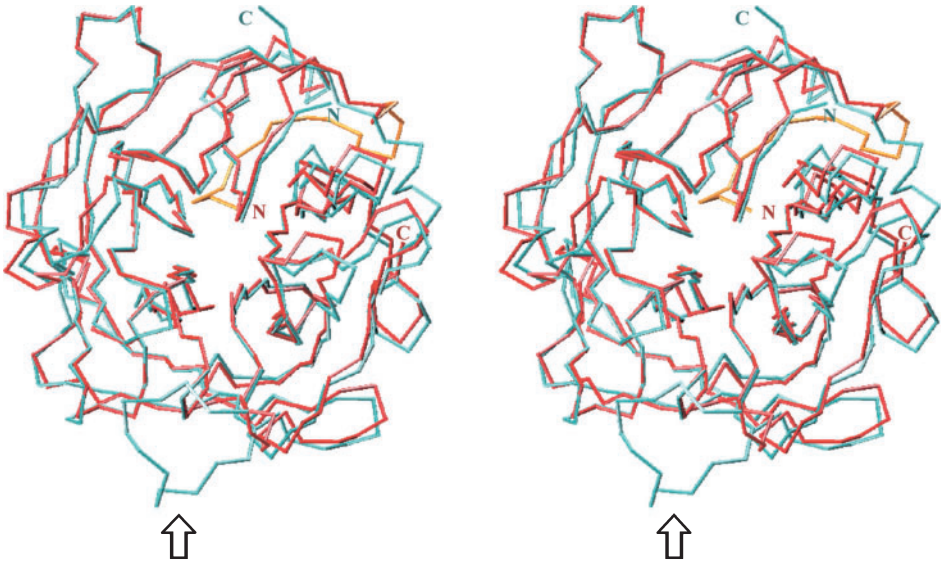

Fig. 3. **Comparison of the C$^{\alpha}$ traces for ABN-TS (red) and *C. japonicus* Arb43A (cyan).** The N-terminal 16 amino acid residues (Val2–Trp17) of ABN-TS are shown in orange. The arrow indicates the loop structure of Arb43A. Superimpositioning was performed using program LSQKAB in the CCP4 suite. The figure was drawn using program VMD (*27*).

activities (*28*), is blocked at one end by a large loop structure composed of 13 amino acid residues between the third and fourth propeller blades (*14*), as indicated by the arrow in Fig. 3. The loop was considered to be responsible for the arabinan-degrading activity of Arb43A for both the endo- and exo-modes of action without any conformational change in the cleft. On the other hand, ABN-TS has only a small loop composed of four amino acid residues, from Glu194 to Asn197, at the location corresponding to that in Arb43A. Thus, the cleft is open on both sides. ABN-TS is a typical endo-acting enzyme (*8*). The "open" structure is suitable for the random binding of several sugar units in a polymeric substrate. Davies and Henrissat reported that this type of cleft is commonly found in endo-acting polysaccharidases (*29*).

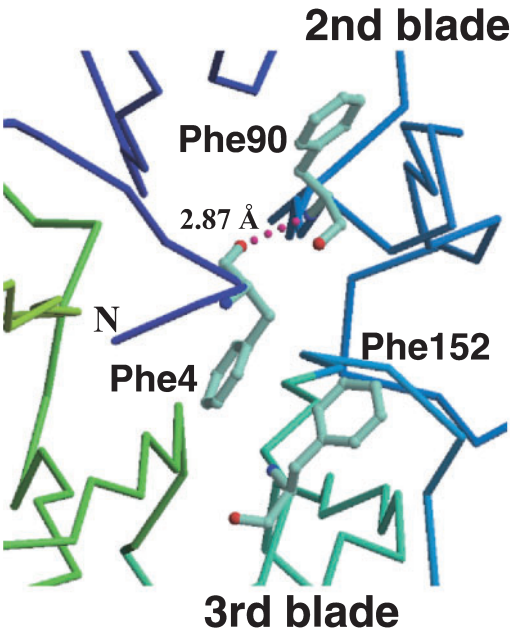

Fig. 4. **Structure of ABN-TS around Phe4 in the N-terminus. Phe4, Phe90 and Phe152 are shown as a ball-and-stick model.** The C$^{\alpha}$ trace of each blade is shown in a different color. The hydrogen bond is shown as a dashed line. This figure was drawn using programs MOLSCRIPT (*23*) and Raster3D (*24*).

Structural Insight into the Thermostability—The β-propeller fold is based on 4- to 8-fold repeats of a four-stranded antiparallel β-sheet motif. One of the remarkable features of the β-propeller fold is that the N- and C-termini are linked to form a closed circle (*30*). A typical example of such a ring closure-mode is found in the structure of the β subunit of heterotrimeric G protein, in which the last four-stranded β-sheet is completed by the incorporation of a strand from the N-terminus (*31*). This arrangement is called "Verclo" and is considered to be needed to stabilize the circular structure of the β-propeller (*32–34*).

In ABN-TS, the fifth blade is composed of the C-terminal residues. Thus, instead of the classical "Verclo" arrangement, ABN-TS exhibits a new closure-mode in the β-propeller, which is composed of the N-terminal residues, with Phe7 to Gly21 located between the first and last blades (Fig. 1a): the N-terminal residues exhibit hydrogen bonds and hydrophobic interactions with the two blades. The residues in the N-terminal region act as an adhesive to close the circle of the β-propeller. In addition, the Phe4 residue is located in the center of the "bottom" face and links the second and third blades through a hydrogen bond and an aromatic stacking interaction, respectively, as shown in Fig. 4.

A mutant, ABN-TS-M, lacking 16 amino acid residues (Val2–Trp17) from the N-terminus of ABN-TS was prepared to confirm the role of the N-terminal residues in the thermostability. The molecular mass of the mutant was estimated to be 33 kDa by SDS-PAGE. ABN-TS-M showed optimal activity at 343 K and pH 6.0, the same as ABN-TS. The wild-type ABN-TS retained more than 80% of its activity even after 4 h at 343 K (Fig. 5). On the other hand, no activity was found for ABN-TS-M after 5 m at 343 K (data not shown). The activity was only 30% that of a control after 5 m at 338 K. Even at 333 K, only 35% of the activity of ABN-TS-M remained after 4 h. The half-life of ABN-TS was 4 h at 348 K, whereas the half-lives of

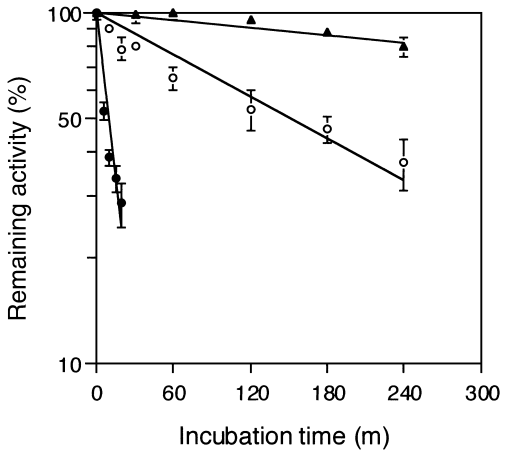

Fig. 5. **Thermostability of the wild-type ABN-TS and mutant ABN-TS-M.** The residual ABN activity was measured after incubation at 343 K for ABN-TS (solid triangles), and 338 K (solid circles) and 333 K for ABN-TS-M (open circles) for various times. The activity value before the start of incubation under each set of conditions was taken as a reference.

ABN-TS-M were 6 min and 2.5 h at 338 and 333 K, respectively. Apparently, deletion of the N-terminal 16 amino acids caused the instability. Therefore, we concluded that the N-terminus plays an important role in the thermostability of ABN-TS.

A current working hypothesis is that thermophilic enzymes are more rigid than their mesophilic homologues at temperatures optimal for the activity of the mesophilic enzymes (298 to 323 K), and that the rigidity is a prerequisite factor for high thermostability (*13*). In this study, we revealed the importance of the N-terminal region for the thermostability of enzymes having β-propeller folds based on the structure of ABN-TS. The structural information presented here should be useful for designing molecules having a new closure-mode to make the β-propeller rigid to increase the thermostability.

The synchrotoron-radiation experiments were performed at the BL40B2 station of SPring-8 with the approval of the Japan Synchrotron Radiation Research Institute (JASRI; Proposal No. 2003B0603-NL1-np). We thank Dr. M. Miura of JASRI for her help with the data collection.

REFERENCES

1. Bacic, A., Harris, P.J., and Stone, B.A. (1988) Structure and function of plant cell walls. *The Biochemistry of Plants* (Preiss, J., eds.) Vol. **14**, pp. 297–371, Academic Press, New York
2. Henrissat, B. and Bairoch, A. (1996) Updating the sequence-based classification of glycosyl hydrolases. *Biochem. J.* **316**, 695–696
3. Coutinho, P.M. and Henrissat, B. (2004) *Carbohydrate-Active Enzymes Server*, http://afmb.cnrs-mrs.fr/~cazy/CAZY/index.html
4. Henrissat, B. and Davies, G. (1997) Structural and sequence-based classification of glycoside hydrolases. *Curr. Opin. Struct. Biol.* **7**, 637–644
5. Voragen, A.G.J., Rombouts, F.M., Searle-van Leeuwen, M.F., Schols, H.A., and Pilnik, W. (1987) The degradation of arabinans by endo-arabinanase and arabinofuranosidases purified from *Aspergillus niger*. *Food Hydrocolloids* **1**, 423–437
6. Seri, K., Sanai, K., Matsuo, N., Kawakubo, K., Xue, C., and Inoue, S. (1996) L-Arabinose selectively inhibits intestinal sucrase in an uncompetitive manner and suppresses glycemic response after sucrose ingestion in animals. *Metabolism* **45**, 1368–1374
7. Takao, M., Yamaguchi, A., Yoshikawa, K., Terashita, T., and Sakai, T. (2002) Molecular cloning of the gene encoding thermostable endo-1, 5-α-L-arabinase of *Bacillus thermodenitrificans* TS-3 and its expression in *Bacillus subtilis*. *Biosci. Biotechnol. Biochem.* **66**, 430–433
8. Takao, M., Akiyama, K., and Sakai, T. (2002) Purification and characterization of thermostable endo-1, 5-α-L-arabinase from a strain of *Bacillus thermodenitrificans*. *Appl. Environ. Microbiol.* **68**, 1639–1646
9. Van den Burg, B., Vriend, G., Veltman O.R., Venema, G., and Eijsink, V.G.H. (1998) Engineering an enzyme to resist boiling. *Proc. Natl Acad. Sci. USA* **95**, 2056–2060
10. Bogin, O., Peretz, M., Hacham, Y., Korkhin, Y., Frolow, F., Kalb (Gilboa), A.J., and Burstein, Y. (1998) Enhanced thermal stability of *Clostridium beijerinckii* alcohol dehydrogenase after strategic substitution of amino acid residues with prolines from the homologous thermophilic *Thermoanaerobacter brockii* alcohol dehydrogenase. *Protein Sci.* **7**, 1156–1163
11. Russell, R.J.M., Ferguson, J.M.C., Hough, D.W., Danson, M.J., and Taylor, G.L. (1997) The crystal structure of citrate synthase from the hyperthermophilic archaeon *Pyrococcus furiosus* at 1.9 Å resolution. *Biochemistry* **36**, 9983–9994
12. Vieille, C. and Zeikus, G.J. (1996) Thermozymes: identifying molecular determinants of protein structural and functional stability. *Trends Biotechnol.* **14**, 183–190
13. Vieille, C. and Zeikus, G.J. (2001) Hyperthermophilic enzymes: sources, uses, and molecular mechanisms for thermostability. *Microbiol. Rev.* **65**, 1–43
14. Nurizzo, D., Turkenburg, J.P., Charnock, S.J., Roberts, S.M., Dodson, E.J., McKie, V.A., Taylor, E.J., Gilbert, H.J., and Davies, G.J. (2002) *Cellvibrio japonicus* α-L-arabinanase 43A has a novel five-blade β-propeller fold. *Nat. Struct. Biol.* **9**, 665–668
15. Yamaguchi, A., Tada, T., Nakaniwa, T., Kitatani, T., Takao, M., Sakai, T., and Nishimura, K. (2004) Crystallization and preliminary X-ray diffraction analysis of a thermostable endo-1, 5-α-L-arabinanase from *Bacillus thermodenitrificans* TS-3. *Acta Cryst.* **D60**, 1149–1151
16. Otwinowski, Z. and Minor, W. (1997) Processing of X-ray diffraction data collected in oscillation mode. *Methods Enzymol.* **276**, 307–326
17. Navaza, J. (1994) *AMoRe*: an automated package for molecular replacement. *Acta Cryst.* **A50**, 157–163
18. Collaborative Computational Project, Number 4 (1994) The *CCP*4 suite: programs for protein crystallography. *Acta Cryst.* **D50**, 760–763
19. Brünger, A.T., Adams, P.D., Clore, G.M., DeLano, W.L., Gros, P., Grosse-Kunstleve, R.W., Jiang, J.-S., Kuszewski, J., Nilges, M., Pannu, N.S., Read, R.J., Rice, L.M., Simonson, T., and Warren, G.L. (1998) Crystallography & NMR system: A new software suite for macromolecular structure determination. *Acta Cryst.* **D54**, 905–921
20. Jones, T.A., Zou, J.-Y., Cowan, S.W., and Kjeldgaard, M. (1991) Improved methods for building protein models in electron density maps and the location of errors in these models. *Acta Cryst.* **A47**, 110–119
21. Laskowski, R.A., MacArthur, M.W., Moss, D.S., and Thornton, J.M. (1993) *PROCHECK*: a program to check the stereochemical quality of protein structures. *J. Appl. Crystallogr.* **26**, 283–291
22. Somogyi, M. (1952) Notes on sugar determination. *J. Biol. Chem.* **195**, 19–23
23. Kraulis, P.J. (1991) MOLSCRIPT: a program to produce both detailed and schematic plots of protein structures. *J. Appl. Crystallogr.* **24**, 946–950
24. Merritt, E.A. and Bacon, D.J. (1997) Raster3D: photorealistic molecular graphics. *Methods Enzymol.* **277**, 505–524

25. DINO: Visualizing Structural Biology (2001) http://www.dino3d.org
26. Pons, T., Naumoff, D.G., Martínez-Fleites, C., and Hernández, L. (2004) Three acidic residues are at the active site of a β-propeller architecture in glycoside hydrolase families 32, 43, 62, and 68. *Proteins* **54**, 424–432
27. Humphrey, W., Dalke, A., and Schulten, K. (1996) VMD: visual molecular dynamics. *J. Mol. Graph.* **14**, 33–38
28. McKie, V.A., Black, G.W., Millward-Sadler, S.J., Hazlewood, G.P., Laurie, J.I., and Gilbert, H.J. (1997) Arabinanase A from *Pseudomonas fluorescens* subsp. *cellulosa* exhibits both an endo- and exo-mode of action. *Biochem. J.* **323**, 547–555
29. Davies, G., and Henrissat, B. (1995) Structures and mechanisms of glycosyl hydrolases. *Structure* **3**, 853–859
30. Fülöp, V. and Jones, D.T. (1999) β propellers: structural rigidity and functional diversity. *Curr. Opin. Struct. Biol.* **9**, 715–721
31. Sondek, J., Bohm, A., Lambright, D.G., Hamm, H.E., and Sigler, P.B. (1996) Crystal structure of a G_A protein βγ dimmer at 2.1 Å resolution. *Nature* **379**, 369–374
32. Baker, S.C., Saunders, N.F.W., Willis, A.C., Ferguson, S.J., Hajdu, J., and Fülöp, V. (1997) Cytochrome cd_1 structure: unusual haem environments in a nitrite reductase and analysis of factors contributing to β-propeller folds. *J. Mol. Biol.* **269**, 440–455
33. Beisel, H.-G., Kawabata, S., Iwanaga, S., Huber, R., and Bode, W. (1999) Tachylectin-2: crystal structure of a specific GlcNAc/GalNAc-binding lectin involved in the innate immuneity host defense of the Japanese horseshoe crab *Tachypleus tridentatus*. *EMBO J.* **18**, 2313–2322
34. Jawad, Z. and Paoli, M. (2002) Novel sequences propel familiar folds. *Structure* **10**, 447–454